Ab Initio and Experimental Studies of the Large-Amplitude Motion in BF_2OH

Laurent H. Coudert,*,† Pablo Garcia-Fernandez,‡ Heinrich Mäder,§ Jean Demaison,⊥ and James E. Boggs‡

LISA, CNRS UMR 7583, Universités Paris 12 et Paris 7, CNRS, 61 Avenue du Général de Gaulle, F-94010 Créteil, France; Department of Chemistry, University of Texas, Austin, Texas 78712; Institut für Physikalische Chemie, Universtät Kiel, Olshausenstr. 40, D-24098 Kiel, Germany; and Laboratoire de Physique des Lasers, Atomes et Molécules, UMR CNRS 8523, Bat. P5, Université de Lille I, 59655 Villeneuve d'Ascq Cedex, France

Received: October 19, 2007; In Final Form: December 2, 2007

The ground state rotational spectrum of BF_2OH was measured under high resolution by microwave Fourier transform spectroscopy (FTMW), and the small torsional splitting could be resolved for several lines. This splitting was analyzed using a phenomenological model previously developed for HNO_3 [Coudert and Perrin, *J. Mol. Spectrosc.* **1995**, *172*, 352] and with the help of the geometries of the stationary points calculated ab initio. The torsional splitting was also calculated using the results of the calculations for the ground vibrational state, for the excited OH torsional states 9^1 and 9^2, and for the excited BOH bending state 4^1, and a satisfactory agreement with available experimental data was found.

1. Introduction

BF_2OH, difluoroboric acid, is a reactive intermediate in the hydrolysis of BF_3. The equilibrium geometry and harmonic force field have been calculated at the coupled cluster level of theory including a perturbational estimate of the effects of connected triple excitations [CCSD(T)].[1] The matrix infrared (IR) spectra of eight isotopologues were first observed by Jacox et al.[2] The first high-resolution IR spectrum of BF_2OH in the gas phase was observed by Collet et al.[3] using a Fourier transform spectrometer. Analyses of the ν_8 and ν_9 fundamental bands of ^{11}B located at 684.160 and 522.870 cm^{-1}, respectively, were performed. Later on, the ν_5, ν_8, ν_9, and $\nu_8 + \nu_9$ bands of ^{10}B and ν_7, ν_5, and $\nu_8 + \nu_9$ bands of ^{11}B were analyzed for the first time up to very high rotational quantum numbers.[4] For both isotopic species and for all bands, the maximum J values ranges from 44 to 64.

The microwave spectrum was first measured by Takeo and Curl.[5] Later, Vorman and Dreizler[6] measured the microwave Fourier transform (FTMW) spectra of three isotopologues of BF_2OH ($^{11}BF_2OH$, $^{11}BF_2OD$, and $^{11}BF_2{}^{18}OH$) and derived accurate quadrupole coupling constants for ^{11}B. Recently, the millimeter-wave spectra of the ^{11}B and ^{10}B isotopologues were measured in their ground vibrational state.[1] As a result, accurate ground state rotational and centrifugal distortion constants were determined for these isotopic species. However, the observed minus calculated frequency of the FTMW lines was found to be almost 2 orders of magnitude larger than their stated precision (3 kHz). It was checked in the present work that the measurements of Vorman and Dreizler are accurate and that their analysis is correct.

To explain this surprising result, it is interesting to compare BF_2OH to its isoelectronic molecule $HONO_2$ (nitric acid). For HNO_3, the ν_9 mode (torsion of the OH bond relative to the NO_2 moiety) is a large-amplitude motion. This induces a splitting of the energy levels which is observable in the infrared spectrum as well as in the rotational spectrum.[7] Therefore, the occurrence of large-amplitude torsional splittings might be expected in BF_2OH, too. Indeed, the IR spectra of the $2\nu_9$ and ν_4 bands were recently analyzed under high resolution,[8] and a splitting of 0.005 and 0.0035 cm^{-1} was observed for the energy levels of the 9^2 and 4^1 states, respectively. Thus, a splitting might also be observed in the rotational spectrum. To check this point, we have remeasured by FTMW the ground state rotational spectrum of $^{11}BF_2OH$, and we have indeed found a torsional splitting for most lines (see Figure 1).

To get a better understanding of the large-amplitude motion, we have calculated ab initio the potential surface along the minimum-energy path of the internal rotation. Furthermore, in order to improve the fit of the experimental splittings, it is very useful to have the equilibrium structure of the transition state which can only be determined by ab initio methods. Finally, the phenomenological model we use to fit the splittings does not allow us to determine the tunneling splittings. For this reason, we have calculated it ab initio. In the last part of this paper the accuracy of this ab initio prediction is discussed using the available experimental information.

2. Ab Initio Potential and Associated Vibronic Functions

2.1. Computational Details. The simulation of the internal rotation in BF_2OH requires accurate knowledge of the geometry, energy, and frequencies of this molecule at the stationnary points of the energy surface as well as along the minimum-energy path connecting them. In order to achieve this goal, we have used three methods of electronic structure calculation: (i) the Kohn−Sham density functional theory[9] using Becke's three-parameter hybrid exchange functional[10] and the Lee−Yang−Parr correlation functional,[11] together denoted as B3LYP; (ii) second-order Møller−Plesset perturbation theory (MP2);[12] and (iii) the coupled-cluster (CC) method with single and double excitations (CCSD)[13] augmented by a perturbational estimate of the effects of connected tripe excitations [CCSD(T)].[14] B3LYP calculations were carried out using the MOLPRO program system[15] while

* Author to whom correspondence should be addressed. E-mail: coudert@lisa.univ-paris12.fr.
† Universités Paris 12 et Paris 7.
‡ University of Texas.
§ Universtät Kiel.
⊥ Université de Lille I.

10.1021/jp709852p CCC: $40.75
Published on Web 01/31/2008

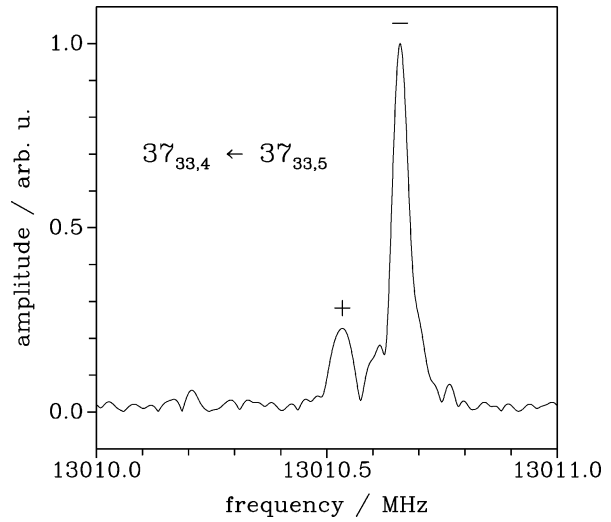

Figure 1. Trace of the $37_{33,4} \leftarrow 37_{33,5}$ rotational transition. Its two tunneling components can clearly be seen. The strong one is at 13 010.66 MHz and the weak one at 13 010.53 MHz.

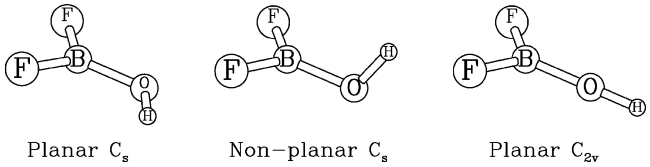

Figure 2. Equilibrium geometries of BF_2OH relevant in the calculation of the internal rotation of the BF_2 group with respect to the OH (see text).

MP2 and CCSD(T) results were obtained using a local version of the ACES2 package.[16] The implementation of first and second analytic derivatives in the last program makes the calculation of accurate force fields, which include cubic and quartic corrections, computationally accessible even at the CCSD(T) level. We have employed Dunning's correlation consistent basis sets cc-pV*X*Z ($X = 3, 4$)[17] for all our calculations. The computational benchmark of geometries carried out by Bak et al.[18] indicates that distances and angles obtained at the CCSD-(T)/cc-pVQZ level differ, typically, from experimental ones by no more than 0.3 pm and 0.5°, respectively.

We have considered three possible equilibrium geometries that may participate in the internal rotation of the BF_2 group with respect to the OH group. These configurations, which can be conveniently characterized by the point group to which they belong, are the high-symmetry C_{2v} configuration, the planar C_s minimum, and the C_s transition state (see Figure 2). Their respective optimized geometric parameters and energies above the minimum for the different calculation methods are given in Tables 1−3. We find that the geometries obtained through MP2 and CCSD(T) are very similar, differing usually by 1−2 pm and 0.1°, while the differences with those calculated using B3LYP are slightly larger. Moreover, when going from cc-pVTZ to cc-pVQZ, we find similarly small differences in geometry. The only exception is the BOH angle, which is ∼0.3° larger with the larger basis. However, this difference is still small, and we can regard the geometry as converged. Our final geometries are in agreement with those presented by Breidung et al.[1] where a more detailed analysis of the effect of the basis size on the geometry can be found.

When the vibrational frequencies are calculated, it is found that the high-symmetry configuration presents two imaginary modes; the nonplanar C_s structure gives one while the planar C_s form is stable. The instability of one of the modes of the high-symmetry configuration (Q_9) leads to the planar minimum while the other (Q_4) to the nonplanar C_s structure, which is the transition state between the two equivalent global minimum configurations. The harmonic vibrational frequencies at the minimum (Table 4) present significant differences from the corresponding experimental ones,[2−4] particularly for Q_1, Q_4, and Q_9 where relative errors of ∼5% are found. Using the previous results, this can be easily understood since those modes are the ones more involved in the internal rotation of BF_2OH. It is seen (Table 4) that when the force field's cubic and quartic terms are taken into account, the resulting vibrational frequencies are in much closer agreement with experiment (with relative errors smaller than 0.5%).

2.2. Tunneling Splitting Calculation. We have calculated the minimum-energy path (MEP) existing between the minimum and transition state by fixing the angle (ϕ) between the planes containing F_1BF_2 and BOH and optimizing the rest of the coordinates. Considering the C_{2v} equilibrium configuration as the reference geometry, we can describe the MEP in terms of the normal modes at this geometry. This is shown in Table 5 where it can be seen that even though all normal modes participate in the distortion, Q_4 and Q_9 are, as could be expected, the dominant ones. Fitting the MEP using a potential varying as cos 2ϕ (see Figure 3) and employing elliptic coordinates to take into account the significant variation in momentum of inertia of the OH group at the minimum and transition state due to the difference existing between Q_4 ($\phi = 90$) and Q_9 ($\phi = 0$), we solve the Schrödinger equation associated with the (internal) rotation coordinate of the BF_2 group with respect to the OH group and use the resulting energy levels to estimate the tunneling splitting in BF_2OH when $J = 0$ to be $\sim 6 \times 10^{-6}$ cm^{-1}.

Perrin et al.[8] found a splitting of 0.0038 and 0.0051 cm^{-1} associated respectively with the 4^1 and 9^2 vibrational excited states. Such tunneling splittings are usually associated with large-amplitude motions like that occurring in ν_9. However, it is not so clear why a similarly large splitting could be also associated with 4^1. In order to describe the motion associated with these two modes and clarify this issue, we use the following pseudo Jahn−Teller (PJT) coupling[19,20] matrix:

$$H = \begin{pmatrix} 0 & F_4Q_4 & F_9Q_9 \\ F_4Q_4 & \Delta_4 & 0 \\ F_9Q_9 & 0 & \Delta_9 \end{pmatrix} + \frac{1}{2}K_4{Q_4}^2 + \frac{1}{2}K_9{Q_9}^2 + G_4{Q_4}^4 + G_9{Q_9}^4 + G_{49}{Q_4}^2{Q_9}^2 \quad (1)$$

where the symbols F_i, K_i, and G_i represent respectively the linear pseudo-Jahn−Teller constant, the force constant, and a quartic correction to the potential along the mode Q_i. G_{49} is the quartic coupling term between Q_4 and Q_9. Finally, Δ_4 and Δ_9 are the electronic excitation energies at the high-symmetry configuration to the states that produce the PJT coupling. Since we just seek to understand the value of the experimental splitting (associated to the shape of the ground state energy surface) and not to give a detailed description of the PJT coupling in BF_2OH, the energies of these excited states have not been calculated. Then, the numerical values for these constants are found by arbitrarily setting $\Delta_4 = \Delta_9$ and adjusting the rest so that the energy (Tables 1−3), at the equilibrium position along the Q_4 and Q_9 coordinates (Table 5) and harmonic vibrational frequencies along Q_4 and Q_9 (Table 4) are perfectly reproduced.

We solve the vibronic problem associated with matrix (1) by projecting the Hamiltonian on a direct product basis of harmonic oscillator functions and diagonalizing the resulting

TABLE 1: Geometry Parameters[a] for the Planar C_s Configuration of BF_2OH (Global Minimum)

method	R(BO)	$R(BF_{trans})$	$R(BF_{cis})$	R(BH)	θ(FBF)	$\theta(F_{cis}BO)$	θ(BOH)
B3LYP/cc-pVTZ	134.90	132.09	133.10	95.37	118.21	122.32	114.39
B3LYP/cc-pVQZ	134.84	131.98	132.98	95.32	118.24	122.29	114.02
MP2/cc-pVTZ	134.78	131.66	132.69	95.85	118.32	122.40	112.59
MP2/cc-pVQZ	134.59	131.47	132.47	95.69	118.39	122.35	112.98
CCSD(T)/cc-pVTZ	134.69	131.49	132.49	95.81	118.32	122.32	112.61
CCSD(T)/cc-pVQZ	134.48	131.28	132.26	95.65	118.38	122.25	113.01

[a] Distances are given in pm and angles in deg.

TABLE 2: Geometry Parameters[a] for the Nonplanar C_s Configuration of BF_2OH (Transition State) and Energy above Global Minimum

method	R(BO)	R(BF)	R(OH)	θ(FBF)	θ(FBO)	θ(BOH)	ΔE
B3LYP/cc-pVTZ	135.58	132.57	95.68	116.56	121.68	121.12	2981
B3LYP/cc-pVQZ	135.51	132.39	95.60	116.61	121.66	120.34	2989
MP2/cc-pVTZ	135.59	132.09	95.50	116.74	121.57	119.32	3117
MP2/cc-pVQZ	135.37	131.90	95.24	116.78	121.55	120.28	3121
CCSD(T)/cc-pVTZ	135.59	131.89	95.43	116.76	121.57	118.98	3120
CCSD(T)/cc-pVQZ	135.43	131.86	95.37	116.78	121.56	120.01	3124

[a] Distances are given in pm, angles in deg, and energies in cm^{-1}.

TABLE 3: Geometry Parameters[a] for the C_{2v} Configuration of BF_2OH (High-Symmetry Configuration) and Energy above Global Minimum

method	R(BO)	R(BF)	R(OH)	θ(FBO)	ΔE
B3LYP/cc-pVTZ	131.50	133.05	94.24	116.42	5038
B3LYP/cc-pVQZ	131.47	132.91	94.15	116.52	5051
MP2/cc-pVTZ	131.10	132.66	93.92	116.48	5238
MP2/cc-pVQZ	131.17	132.40	93.91	116.60	5266
CCSD(T)/cc-pVTZ	130.99	132.47	93.82	116.46	5330
CCSD(T)/cc-pVQZ	131.08	132.20	93.81	116.58	5372

[a] Distances are given in pm, angles in deg, and energies in cm^{-1}.

matrix by the Lanczos method.[21] Also, the exponents of the basis functions are variationally optimized to minimize the energy of the ground state for a given basis size. The final results have been obtained using a basis set containing 35 harmonic oscillator functions for each mode. We have checked that, at this level of calculation, the lowest vibronic levels are converged within 10^{-8} cm^{-1} ($\sim$1 kHz).

The energy levels obtained by our method describe the coupled vibrational-tunneling problem in the ν_4 and ν_9 vibrations including excited states of these modes. A summary of these results is presented in Table 6. There we can observe that although we only fit the model so that the curvature at the bottom of the potential reproduces the harmonic frequencies obtained from ab initio calculations, the resulting excitation energies associated with the ν_4 and ν_9 modes are closer both to the frequencies calculated through the quartic force field and also to the experimental ones.[2-4] Since these modes are those whose frequencies are more strongly changed through the introduction of the quartic force field, we conclude that the internal rotation is the main source of anharmonicity for them. Our best result, at the CCSD(T)/cc-pVQZ level, predicts that the tunneling splitting in the ground state is 2.1×10^{-5} cm^{-1}. Calculations at other levels give moderately different values, which is understandable due to the smallness of δ, the electronic excitation.

2.3. Comparison to Previous IR Results. Experiments have been able to resolve the tunneling splitting in the 4^1 (0.0038 cm^{-1}) and 9^2 (0.0051 cm^{-1}) excited vibrational states.[8] Our calculated values for these splittings using the PJT model and parameters extracted from CCSD(T)/cc-pVQZ calculations are 0.0061 and 0.0043 cm^{-1} for 4^1 and 9^2, respectively. For the 9^1 state no tunneling splitting could be observed,[4] and this is consistent with a calculated value of only 6.2×10^{-4} cm^{-1}, about 10 times smaller than the two previous ones and well below the resolution of an infrared spectrum. Taking into account the smallness of these figures, we consider that the experimental high-resolution data and ab initio calculations are in acceptable agreement. It is also significant to point out that even though only the harmonic frequencies are used to calculate the parameters of eq 1, the resulting frequencies are much closer to the experimental ones, showing that the main source of anharmonicity for ν_4 and ν_9 comes from their mutual coupling.

In order to check the origin of the unexpected value of the splitting for the 4^1 band, we plot the nuclear density associated with the lowest levels of the potential described by eq 1 in Figure 4. As can be immediately appreciated, the levels 4^1 and 9^2 are strongly mixed due to the anharmonicity of the energy surface which explains the value of δ for 4^1. Without this mixing, the wave functions associated with these modes would be far from the MEP (also shown in Figure 4) and their corresponding energies would be higher.

3. Experimental Details

Most of the experimental data used in this paper come from Breidung et al.[1] A few lines were measured more accurately in Kiel, in the frequency range from about 8 to 13 GHz, employing a Fourier transform microwave spectrometer for the X/Ku band with automatic scan facility[22] and a waveguide cell of quadratic cross section and 12 m length.[23] The sample was prepared by filling BF_3 into the waveguide cell which reacted with some residual water to BF_2OH. BF_3 was obtained commercially from Fa. Messer Griesheim, Germany, and used without further purification. Ambient temperature and sample pressures of about 0.06 Pa (0.4 mTorr) were used throughout. The transition frequencies were determined from a peak finder routine of the lines, in most cases at an accuracy of better than 5 kHz.

4. Tunneling−Rotational Energy Levels

An internal axis method (IAM) approach[24-26] was used to account for the tunneling−rotational energy levels of the BF_2OH molecule. This theoretical approach allowed us to model the rotational dependence of the tunneling splitting and was utilized to carry out a line frequency analysis of the microwave data. Values retrieved for the parameters involved in the rotational dependence of the tunneling splitting were compared to those calculated making reasonable assumptions about the

TABLE 4: Calculated Vibrational Frequencies[a] for BF_2OH

method	$Q_1(a')$	$Q_2(a')$	$Q_3(a')$	$Q_4(a')$	$Q_5(a')$	$Q_6(a')$	$Q_7(a')$	$Q_8(a'')$	$Q_9(a'')$
B3LYP/cc-pVTZ	3853	1487	1428	1014	884	478	445	560	684
B3LYP/cc-pVQZ	3821	1495	1422	1016	869	480	445	533	677
MP2/cc-pVTZ	3920	1509	1453	1013	897	487	449	553	699
	3746	*1481*	*1424*	*963*	*885*	*484*	*448*	*523*	*692*
MP2/cc-pVQZ	3904	1500	1449	1017	893	484	448	549	692
	3729	*1477*	*1423*	*963*	*880*	*481*	*447*	*523*	*687*
CCSD(T)/cc-pVTZ	3914	1515	1462	1023	900	488	450	553	701
	3732	*1478*	*1420*	*963*	*884*	*482*	*448*	*524*	*690*
CCSD(T)/cc-pVQZ	3908	1510	1458	1025	899	488	451	551	697
	3718	*1473*	*1419*	*962*	*882*	*480*	*447*	*523*	*685*
experimental	3712.5	1464.3	1414.9	961.5	880.7	479.2	446.5	522.9	684.2

[a] Frequencies are given in cm^{-1}. The use of normal and italic fonts denotes that the frequencies have been obtained respectively in the harmonic approximation and including cubic and quartic corrections in the force field.

TABLE 5: Variation of the Geometry and Energy of BF_2OH along the MEP[a]

ϕ	Q_1	Q_2	Q_3	Q_4	Q_5	Q_6	Q_7	Q_8	Q_9	energy
0	−50.55	−2.09	−15.28	0.	−8.34	0	−2.49	8.36	87.79	0
15	−50.35	−2.14	−13.75	21.54	−7.50	−3.31	−2.26	6.60	82.53	214.6
30	−49.10	−2.27	−11.69	41.25	−5.29	−6.37	−1.76	4.87	73.26	796.9
45	−47.11	−2.45	−8.96	57.54	−2.31	−8.85	−1.12	3.23	58.92	1584.1
60	−44.67	−2.62	−5.97	69.26	0.61	−10.50	−0.52	2.05	40.91	2359.2
75	−42.50	−2.72	−2.96	76.01	2.68	−11.31	−0.10	1.06	20.83	2917.3
90	−42.04	−2.77	0.00	77.90	3.44	−11.49	0.07	0	0	3118.2

[a] The MEP (see text) is expressed in terms of the normal modes of the C_{2v} configuration. Coordinates are given in pm and energy in cm^{-1}.

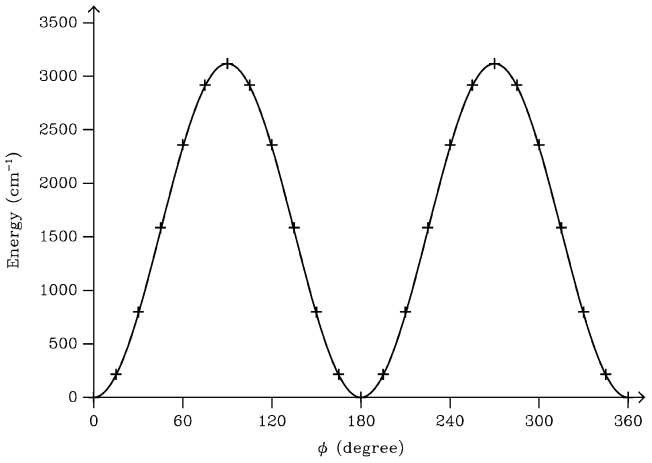

Figure 3. Minimum-energy path as calculated in CCSD(T)/cc-pVQZ and its fit using a cos 2ϕ function.

path along which the molecule tunnels between its two equilibrium configurations.

4.1. Tunneling Matrix Elements. BF_2OH is a nonrigid molecule displaying an internal rotation of its BF_2 group with respect to the OH group. With the help of the theoretical IAM approach,[24−26] we can express the tunneling−rotational energy of this molecule in terms of several effective parameters that are to be determined by data fitting. This IAM approach allows us to account for the rotational dependence of the tunneling splitting, but it does not allow us to predict the value of the tunneling splitting from a potential energy surface.

Applying the IAM approach[24−26] first requires choosing reference coordinates and reference positions for the five atoms of the molecule. This first step has already been carried out in section 3 of Coudert and Perrin.[27] As indicated by eq 1 of this reference, laboratory-fixed Cartesian coordinates of the five atoms depend on the laboratory-fixed coordinates of the molecular center of mass, on the three Eulerian angles χ, θ, ϕ, on the reference positions $\mathbf{a}_i(\gamma)$, which depend explicitly on the large-amplitude angular coordinate γ, and on the infinitesimal vibrational displacement vectors. The atom numbering used in the present work is analogous to the one used in the case of nitric acid;[27,28] the two fluorine atoms exchanged by the large-amplitude motion are numbered 1 and 2, and the boron, oxygen, and hydrogen atoms are numbered 3, 4, and 5, respectively. The reference positions $\mathbf{a}_i(\gamma)$ can be conveniently obtained with the help of vectors $\mathbf{b}_i(\gamma)$ depending on eight structural parameters: four angles α_1, α_2, δ, and θ(BOH) and four distances $R(BF_1)$, $R(BF_2)$, R(BO), and R(OH). Expressions for the five vectors $\mathbf{b}_i(\gamma)$ are displayed in Table 7. As emphasized by this table, α_1 and α_2 are the angles between the direction of the BO bond and the BF_1 and BF_2 bonds, respectively, when the angle δ is zero. The latter angle has a small value and corresponds, when $\alpha_1 = \alpha_2$, to the angle between the previous direction and the one bisecting the BF_1 and BF_2 bonds. When using Table 7, it should be kept in mind that the eight structural parameters depend on the large-amplitude coordinate γ. The reference position vectors are related to the $\mathbf{b}_i(\gamma)$ vectors by the following equation

$$\mathbf{a}_i(\gamma) = R[\mathbf{b}_i(\gamma) - \mathbf{r}_0] \qquad (2)$$

where $\mathbf{r}_0$ is a vector such that the origin of the molecule-fixed axis system is the molecular center of mass for all values of γ and R is a rotation such that this axis system is the principal axis system for $\gamma = 0$ and π. The $\mathbf{r}_0$ vector in eq 2 depends implicitly on the large-amplitude coordinate γ. The R rotation in this equation is a constant rotation about the y-axis such that the x,y,z axes are respectively parallel to the a,c,b axes, for $\gamma = 0$ and π. For these two values of γ, the II^L representation is used.

Like the nitric acid molecule,[27,28] the BF_2OH molecule has two planar equilibrium configurations, numbered 1 and 2, centered around $\gamma = 0$ and π, respectively. These configurations correspond to the planar configuration with C_s symmetry described in section 2.1. There also exists[27,28] an intermediate configuration for the large-amplitude motion, characterized by

TABLE 6: Results of the PJT Model To Calculate the Tunneling Splitting[a] for BF_2OH

	$4^0 9^0$	$4^0 9^1$		$4^1 9^0$		$4^0 9^2$	
method	Δ	$h\nu$	Δ	$h\nu$	Δ	$h\nu$	Δ
MP2/cc-pVTZ	2.9×10^{-5}	525	6.3×10^{-4}	942	6.5×10^{-3}	1109	2.8×10^{-3}
MP2/cc-pVQZ	2.7×10^{-5}	524	6.2×10^{-4}	948	6.4×10^{-3}	1099	3.2×10^{-3}
CCSD(T)/cc-pVTZ	2.3×10^{-5}	525	6.2×10^{-4}	953	6.3×10^{-3}	1110	3.5×10^{-3}
CCSD(T)/cc-pVQZ	2.1×10^{-5}	523	6.2×10^{-4}	955	6.1×10^{-3}	1095	4.3×10^{-3}

[a] Tunneling splitting is calculated when $J = 0$ in the ground and excited vibrational states. Its value is given in cm^{-1} in the columns headed Δ. The vibrational energy is given in cm^{-1} in the columns headed $h\nu$.

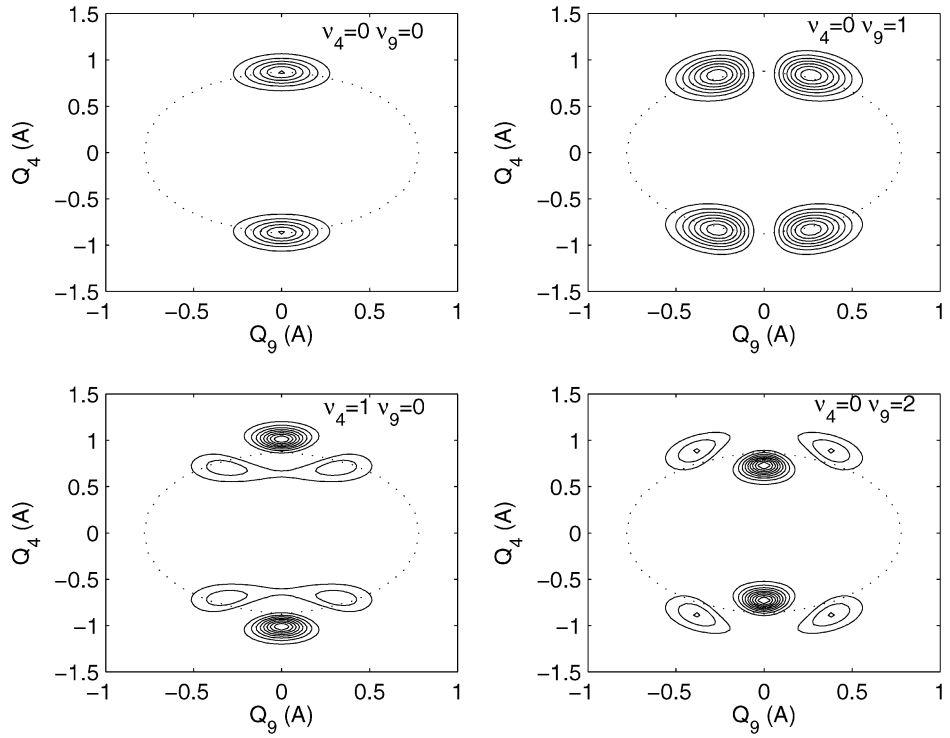

Figure 4. Nuclear densities associated with one of the tunneling components of the ground, 4^1, 9^1, and 9^2 vibrational states. The projection on the MEP on the Q_4 and Q_9 coordinates is shown with a dotted line.

TABLE 7: $b_i(\gamma)$ Vectors[a]

i	$b_i(\gamma)$
1	$R(BF_1)\ C_y(\delta)\cdot C_z(\gamma)\cdot C_y(\alpha_1)\cdot \mathbf{k}$
2	$R(BF_2)\ C_y(\delta)\cdot C_z(\gamma)\cdot C_y(\alpha_2)\cdot \mathbf{k}$
3	0
4	$R(BO)\cdot \mathbf{k}$
5	$\mathbf{b}_4(\gamma) - R(OH)\ C_y(\theta(BOH))\cdot \mathbf{k}$

[a] These vectors, defined in section 4.1, are expressed in terms of five angles α_1, α_2, γ, δ, and θ(BOH) and four distances $R(BF_1)$, $R(BF_2)$, R(BO), and R(OH). $\mathbf{k}$ is the unit vector along the z-axis.

TABLE 8: Numerical Values[a] for Structural Parameters of Various Configurations of BF_2OH[b]

	1	2	intermediate
γ	0	180	90
α_1	120.82	120.82	121.60
α_2	−120.82	−120.82	−121.60
δ	−1.43	−1.43	−3.15
θ(BOH)	113.14	113.14	112.13
$R(BF_1)$	132.29	131.29	131.70
$R(BF_2)$	131.29	132.29	131.70
R(BO)	134.48	134.48	135.40
R(OH)	95.74	95.74	105.70

[a] Bond lengths are in pm and bond angles are in deg. Numerical values were obtained from the best geometry reported by Breidung et al.[1] and from the present work. [b] The columns headed 1 and 2 correspond to the equilibrium configurations 1 and 2, respectively. The column headed intermediate corresponds to the intermediate configuration of the large-amplitude tunneling motion.

$\gamma = \pi/2$, corresponding to a saddle point of the potential energy surface. This intermediate configuration is the nonplanar configuration with C_s symmetry also described in section 2.1. The best geometry reported by Breidung et al.[1] in their Table 1 and the results obtained in section 2.1 of the present paper allow us to obtain numerical values for the above structural parameters for these three configurations. These numerical values are given in Table 8, and Figure 5 shows the corresponding geometries.

In agreement with the IAM approach,[24−26] reference basis wave functions should be chosen to determine tunneling matrix elements. This second step has also been carried out in section 3 of Coudert and Perrin.[27] Because the reference positions chosen in this reference are equivalent from the symmetry stand point to those in the present paper, Table 1 as well as eqs 2−11 and eqs 14 and 15 of Coudert and Perrin[27] can be used in the case of BF_2OH. In these equations, the superscripted υ can be ignored since the present investigation only involves the ground vibrational state. In eq 11, the vibrational energy E_υ should be ignored, too, and the constants A^υ and B^υ should be exchanged to account for the fact that the II^L representation is used in the present investigation. After making these changes, eqs 9 and 10 of Coudert and Perrin[27] can be used to obtain tunneling matrix elements as a function of h_2, the magnitude of the tunneling splitting, and of θ_2 and ϕ_2, the angles describing its rotational dependence. These angles parametrize[27] the rotation

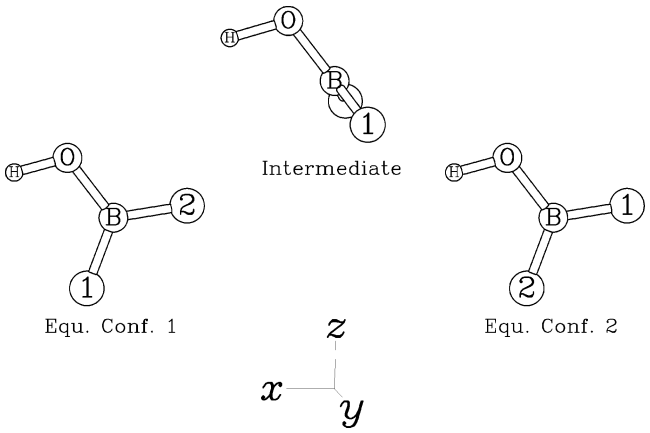

Figure 5. Two equivalent isoenergetic equilibrium configurations of BF_2OH, numbered 1 and 2, and the intermediate configuration of the large-amplitude internal rotation motion. These three configurations are described in section 4.1. The molecule-fixed *xyz*-axis system is drawn at the bottom of the picture for clarity. The angle between the BO bond and the *z*-axis is 38.68°.

$S^{-1}(\phi_2 + \pi,\theta_2,\phi_2)$, where S^{-1} is the direction cosine matrix defined in eq 18 of Hougen,[24] required to cancel the angular momentum generated along the tunneling path.[24−26] Just as in Coudert and Perrin,[27] symmetry-adapted linear combinations of reference wave functions are used and are defined using eq 14 of this reference. These symmetry-adapted linear combinations are denoted $\Psi^{\pm}_{JK\alpha}$ and allow us to block diagonalize the tunneling−rotational Hamiltonian matrix into four blocks corresponding to the four symmetry species of G_4. Their overall symmetry species depend on their rotational symmetry species in the C_s symmetry group of the equilibrium configuration of the molecule. As stated in Coudert and Perrin,[27] this rotational symmetry species is A' when $\alpha = (-1)^{J+K}$ and A'' when $\alpha = -(-1)^{J+K}$. The overall symmetry species in G_4 of a $\Psi^{+}_{JK\alpha}$ wave function is then A_1 (A_2) for A' (A'') rotational symmetry species. For a $\Psi^{-}_{JK\alpha}$ wavefunction, it is B_2 (B_1) for A' (A'') rotational symmetry species. When using symmetry-adapted wave functions, eq 15 of Coudert and Perrin[27] should be used to obtain nonvanishing matrix elements of the tunneling−rotational Hamiltonian.

Tunneling−rotational energy levels obtained after diagonalizing the Hamiltonian matrix will be assigned using the usual rotational quantum number JK_aK_c and the ± sign corresponding to the symmetry-adapted wave function. Since rotational levels with an even (odd) K_c value belong to the symmetry species A' (A'') of C_s, the overall symmetry species of a tunneling-rotational energy level can be determined using the results in the previous paragraph. A schematic energy level diagram where the levels are identified using this labeling scheme can be obtained from the one given for nitric acid in Figure 1 of Coudert and Perrin.[27] The ± sign should be added to the tunneling sublevels so that the upper (lower) tunneling sublevel is a −(+) tunneling−rotational energy level.

Figure 6 shows plots of the tunneling splitting, defined as the energy difference $E^{-}_{JK_aK_c} - E^{+}_{JK_aK_c}$, for the $J_{0,J}$, $J_{1,J}$, and $J_{J,0}$ rotational levels. Tunneling−rotational energies were calculated using eqs 9−11 and 15 of Coudert and Perrin[27] and taking for the spectroscopic constants values close to the actual ones, reported in section 4.2. Values of 10 320, 10 099, and 5095 MHz were taken for the rotational constants, the angles θ_2 and ϕ_2 were set to 80 and 1.8, respectively, and h_2 was assumed to be −0.1 MHz. Figure 6 emphasizes that for the low-lying $J_{0,J}$ and $J_{1,J}$ rotational levels the tunneling splitting becomes constant

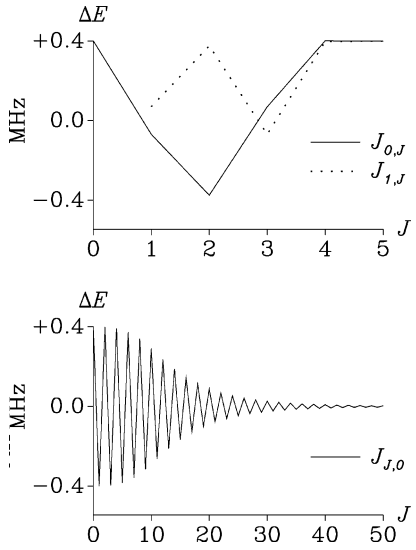

Figure 6. Tunneling splitting as a function of J for three different rotational levels. The upper part of the figure correspond to the cases of the $J_{0,J}$ (solid line) and $J_{1,J}$ (dashed line) rotational levels. The lower part of the figure correspond to the case of $J_{J,0}$ level. In all three cases the difference $\Delta E = E^{+}_{JK_aK_c} - E^{-}_{JK_aK_c}$ is plotted.

for $J > 3$. This result is in agreement with eq 24 of Coudert and Perrin[27] and is due to the fact that the BF_2OH molecule is almost an oblate top. For the high-lying $J_{J,0}$ rotational level, the tunneling splitting displays a fast $(-1)^J$ variation superimposed on a slower one.

4.2. Analysis. The microwave data recorded in the present investigation were analyzed calculating the tunneling−rotational energy with the theoretical approach described in the previous section. As it was not possible to resolve the tunneling splitting for many transitions, the following procedure was adopted. Assuming that two such transitions are assigned as $J'K'_aK'^{+}_c \leftarrow J''K''_aK''^{+}_c$ and $J'K'_aK'^{-}_c \leftarrow J''K''_aK''^{-}_c$, their frequency was calculated as $(E^{+}_{J'K'_aK'_c} + E^{-}_{J'K'_aK'_c} - E^{+}_{J''K''_aK''_c} - E^{-}_{J''K''_aK''_c})/2$, and they were treated as only one transition. In the analysis, transitions were given a weight equal to the inverse of the square of their experimental uncertainty. Table 9 lists assignments, observed frequencies, and observed minus calculated differences for the 236 transitions assigned in this work. The root-mean-square deviation of the observed minus calculated difference is 0.038 MHz, and the unitless standard deviation is 0.58. Table 10 gives the value of the parameters determined in the analysis and their uncertainty. In this table, the parameters h_{2k} and h_{2j}, not used in the case of nitric acid,[27,28] correspond to a distortion-like dependence of the magnitude of the tunneling splitting and are such that in eq 9 of Coudert and Perrin[27] h_2 should be replaced by

$$h_2 + \frac{1}{2}(K'^2 + K''^2)h_{2k} + J(J+1)h_{2j} \qquad (3)$$

4.3. Interpretation of the Spectroscopic Parameters. The angles θ_2 and ϕ_2, determined through fitting in the previous section, can also be calculated theoretically solving eqs 49 of Hougen[24] or eqs 7 and 8 of Coudert and Hougen.[25] These equations allow us to obtain the rotation of the whole molecule required to cancel the angular momentum generated along the tunneling path. Such a calculation was carried out for two different tunneling paths.

For the first tunneling path, which will be referred to as path I, the large-amplitude coordinate γ goes from 0 to π. The eight

TABLE 9: Assignments,[a] Observed Frequencies,[b] and Observed Minus Calculated Differences[c] in the Microwave Spectrum of BF_2OH

J'	K'_a	K'_c	±	J''	K''_a	K''_c	±	obs[b]	diff[c]	J'	K'_a	K'_c	±	J''	K'_a	K'_c	±	obs[b]	diff[c]
1	1	0	−	1	1	1	−	5004.109(20)	32	1	0	1	+	0	0	0	+	15194.673(20)	−11
31	28	3	±	31	28	4	±	8089.725(20)	22[d]	1	1	1	−	0	0	0	−	15415.413(20)	−4
11	10	1	+	11	10	2	+	8741.660(20)	0	1	1	1	+	0	0	0	+	15415.728(20)	6
11	10	1	−	11	10	2	−	8741.956(20)	3	16	14	2	−	16	14	3	−	16549.930(20)	3
21	19	2	−	21	19	3	−	9230.479(20)	0	16	14	2	+	16	14	3	+	16550.022(80)	28
21	19	2	+	21	19	3	+	9230.562(20)	13	26	23	3	+	26	23	4	+	16856.070(20)	4
30	27	3	+	30	27	4	+	9619.547(10)	−26	26	23	3	−	26	23	4	−	16856.169(20)	−10
30	27	3	−	30	27	4	−	9619.610(10)	0	15	13	2	+	15	13	3	+	17940.781(20)	−20
10	9	1	−	10	9	2	−	9722.289(20)	11	15	13	2	−	15	13	3	−	17940.904(20)	8
10	9	1	+	10	9	2	+	9722.591(20)	17	25	22	3	−	25	22	4	−	18799.673(20)	−1
20	18	2	+	20	18	3	+	10655.278(20)	−30	25	22	3	+	25	22	4	+	18799.792(20)	−11
20	18	2	−	20	18	3	−	10655.347(20)	−5	14	12	2	−	14	12	3	−	19252.044(40)	9
9	8	1	+	9	8	2	+	10662.584(20)	16	14	12	2	+	14	12	3	+	19252.192(40)	34
9	8	1	−	9	8	2	−	10662.871(20)	6	17	16	1	±	17	15	2	±	19362.310(80)	−14[d]
29	26	3	−	29	26	4	−	11287.017(10)	9	7	7	1	−	7	5	2	−	19380.045(20)	−3
29	26	3	+	29	26	4	+	11287.092(10)	27	7	7	1	+	7	5	2	+	19380.338(40)	25
8	7	1	−	8	7	2	−	11544.825(20)	−4	18	16	2	±	18	15	3	±	19444.261(80)	−33[d]
8	7	1	+	8	7	2	+	11545.122(20)	−5	19	17	2	±	19	16	3	±	19615.972(80)	3[d]
19	17	2	−	19	17	3	−	12127.300(80)	1	13	11	2	−	13	11	3	−	20464.026(20)	1
7	6	1	+	7	6	2	+	12354.749(20)	−3	24	21	3	+	24	21	4	+	20734.276(20)	−9
7	6	1	−	7	6	2	−	12355.054(20)	2	24	21	3	−	24	21	4	−	20734.432(20)	2
10	9	1	±	10	8	2	±	12838.345(80)	59[d]	8	8	1	+	8	6	2	+	20847.027(40)	−21
37	33	4	+	37	33	5	+	13010.535(10)	3	8	8	1	−	8	6	2	−	20847.315(40)	20
37	33	4	−	37	33	5	−	13010.660(10)	−3	14	12	2	±	14	11	3	±	20859.687(80)	−82[d]
28	25	3	+	28	25	4	+	13068.283(20)	11	13	11	2	±	13	10	3	±	21534.827(80)	85[d]
28	25	3	−	28	25	4	−	13068.339(10)	−10	12	10	2	−	12	10	3	−	21558.788(40)	18
6	5	1	−	6	5	2	−	13081.160(5)	−2	12	10	2	+	12	10	3	+	21558.973(40)	24
6	5	1	+	6	5	2	+	13081.477(10)	14	11	9	2	+	11	9	3	+	22522.045(40)	25
12	11	1	±	12	10	2	±	13467.005(80)	53[d]	11	9	2	−	11	9	3	−	22522.231(40)	4
18	16	2	−	18	16	3	−	13618.383(80)	−4	23	20	3	−	23	20	4	−	22629.538(20)	1
5	4	1	+	5	4	2	+	13715.550(40)	−23	23	20	3	+	23	20	4	+	22629.704(20)	6
5	4	1	−	5	4	2	−	13715.862(40)	−13	10	8	2	−	10	8	3	−	23342.949(20)	23
27	24	3	−	27	24	4	−	14934.964(20)	−3	10	8	2	+	10	8	3	+	23343.142(20)	−18
27	24	3	+	27	24	4	+	14935.080(40)	18	19	18	1	±	19	17	2	±	23503.757(80)	37[d]
2	1	1	−	2	1	2	−	15012.431(20)	3	9	7	2	+	9	7	3	+	24016.395(80)	26
2	1	1	+	2	1	2	+	15012.660(80)	−72	9	7	2	−	9	7	3	−	24016.622(20)	−5
14	13	1	±	14	12	2	±	15033.900(80)	28[d]	22	19	3	+	22	19	4	+	24456.593(80)	−16
17	15	2	+	17	15	3	+	15101.161(20)	−26	22	19	3	−	22	19	4	−	24456.792(80)	8
17	15	2	−	17	15	3	−	15101.234(20)	8	8	6	2	−	8	6	3	−	24544.340(40)	25
1	0	1	−	0	0	0	−	15194.377(20)	13	8	6	2	+	8	6	3	+	24544.591(40)	−3
7	5	2	+	7	5	3	+	24936.571(40)	46	35	0	35	±	34	0	34	±	361638.143(100)	11[d]
7	5	2	−	7	5	3	−	24936.840(40)	18	34	1	33	±	33	1	32	±	361670.906(100)	−10[d]
3	2	2	±	3	0	3	±	25577.880(80)	−93[d]	33	2	31	±	32	2	30	±	361699.685(100)	−23[d]
31	14	18	±	31	12	19	±	188577.797(100)	9[d]	32	3	29	±	31	3	28	±	361725.184(100)	−7[d]
16	2	14	±	15	2	13	±	188587.467(100)	96[d]	31	4	27	±	30	4	26	±	361748.093(100)	−18[d]
20	1	20	±	19	1	19	±	208892.858(100)	47[d]	30	6	25	±	29	6	24	±	361769.160(100)	−34[d]
19	1	18	±	18	2	17	±	208927.273(100)	67[d]	29	6	23	±	28	6	22	±	361789.231(100)	−15[d]
31	11	20	±	31	11	21	±	209064.075(100)	100[d]	28	7	21	±	27	7	20	±	361809.121(100)	71[d]
30	11	20	±	30	9	21	±	209127.758(100)	−129[d]	27	8	19	±	26	8	18	±	361829.550(100)	1[d]
17	16	1	±	16	15	2	±	351049.200(100)	−8[d]	26	9	17	±	25	9	16	±	361851.886(100)	−6[d]
34	0	34	±	33	0	33	±	351458.897(100)	−16 [d]	25	10	15	±	24	10	14	±	361877.685(100)	−32[d]
33	1	32	±	32	1	31	±	351491.838(100)	17[d]	24	11	13	±	23	11	12	±	361909.787(100)	−31[d]
32	2	30	±	31	2	29	±	351520.848(100)	−18[d]	23	13	11	±	22	13	10	±	361954.112(100)	2[d]
30	4	26	±	29	4	25	±	351570.243(100)	15[d]	22	13	9	±	21	13	8	±	362026.544(100)	−3[d]
29	5	24	±	28	5	23	±	351592.088(100)	59[d]	42	7	35	±	42	7	36	±	362065.217(100)	22[d]
28	7	22	±	27	7	21	±	351612.947(100)	23[d]	16	14	3	±	15	12	4	±	362173.267(100)	−101[d]
27	7	20	±	26	7	19	±	351633.779(100)	−16[d]	21	15	7	±	20	15	6	±	362182.578(100)	−98[d]
26	8	18	±	25	8	17	±	351655.572(100)	−12[d]	21	14	7	±	20	14	6	±	362187.355(100)	73[d]
25	9	16	±	24	9	15	±	351679.554(100)	−19[d]	41	6	35	±	41	6	36	±	362199.633(100)	45[d]
24	11	14	±	23	11	13	±	351707.687(100)	11[d]	14	8	7	±	13	6	8	±	362303.633(100)	2[d]
23	11	12	±	22	11	11	±	351743.504(100)	0[d]	20	16	5	±	19	16	4	±	362312.661(100)	−29[d]
18	16	3	±	17	15	2	±	352065.035(100)	−33 [d]	20	15	5	±	19	15	4	±	363255.161(100)	37[d]
65	30	35	±	65	30	36	±	358077.385(100)	−76[d]	17	16	1	±	16	14	2	±	364674.558(100)	34[d]
64	30	35	±	64	29	36	±	358286.700(100)	−42[d]	19	17	2	±	18	17	1	±	364766.606(100)	−3[d]
63	28	35	±	63	28	36	±	358492.719(100)	12[d]	18	17	2	±	17	16	1	±	365016.030(100)	76[d]
62	28	35	±	62	26	36	±	358695.456(100)	4[d]	17	15	2	±	16	13	3	±	365117.548(100)	−34[d]
61	27	35	±	61	25	36	±	358894.886(100)	−10[d]	19	16	3	±	18	16	2	±	366471.995(100)	36[d]
60	26	35	±	60	24	36	±	359091.131(100)	58[d]	65	30	36	±	65	29	37	±	368292.365(100)	−34[d]
59	25	35	±	59	23	36	±	359284.053(100)	69[d]	64	29	36	±	64	28	37	±	368506.274(100)	−23[d]
58	24	35	±	58	22	36	±	359473.674(100)	44[d]	62	26	36	±	62	26	37	±	368924.212(100)	35[d]
57	22	35	±	57	22	36	±	359660.037(100)	45[d]	61	26	36	±	61	24	37	±	369128.248(100)	67[d]
56	21	35	±	56	21	36	±	359843.184(100)	71[d]	59	23	36	±	59	23	37	±	369526.320(100)	79[d]
55	20	35	±	55	20	36	±	360022.962(100)	−11[d]	58	22	36	±	58	22	37	±	369720.305(100)	−16[d]
54	19	35	±	54	19	36	±	360199.588(100)	15[d]	22	18	4	±	21	20	1	±	369825.850(100)	−17[d]
53	18	35	±	53	18	36	±	360372.909(100)	−7[d]	57	21	36	±	57	21	37	±	369911.114(100)	19[d]

TABLE 9: (Continued)

J'	K'_a	K'_c	±	J''	K''_a	K''_c	±	obs[b]	diff[c]	J'	K'_a	K'_c	±	J''	K'_a	K'_c	±	obs[b]	diff[c]
52	18	35	±	52	16	36	±	360543.035(100)	6[d]	18	18	1	±	17	17	0	±	369985.003(100)	14[d]
51	17	35	±	51	15	36	±	360709.824(100)	−41[d]	20	17	4	±	19	17	3	±	370795.412(100)	−55[d]
50	15	35	±	50	15	36	±	360873.404(100)	−13[d]	50	14	36	±	50	14	37	±	371153.950(100)	−23[d]
49	14	35	±	49	14	36	±	361033.732(100)	−14[d]	49	13	36	±	49	13	37	±	371318.287(100)	−21[d]
48	14	35	±	48	12	36	±	361190.776(100)	−95[d]	48	12	36	±	48	12	37	±	371479.285(100)	−54[d]
16	12	4	±	15	10	5	±	371571.357(100)	43[d]	55	18	37	±	55	18	38	±	380550.355(100)	−19 [d]
47	11	36	±	47	11	37	±	371637.041(100)	−25[d]	54	17	37	±	54	17	38	±	380735.593(100)	13[d]
46	10	36	±	46	10	37	±	371791.518(100)	28[d]	53	17	37	±	53	15	38	±	380917.427(100)	−41[d]
16	13	4	±	15	11	5	±	371853.801(100)	−68[d]	52	15	37	±	52	15	38	±	381095.853(100)	−66[d]
34	2	32	±	33	2	31	±	371877.906(100)	2[d]	51	14	37	±	51	14	38	±	381270.998(100)	−53[d]
45	9	36	±	45	9	37	±	371942.588(100)	−23[d]	50	13	37	±	50	13	38	±	381442.784(100)	−37[d]
30	6	24	±	29	6	23	±	371964.937(100)	7[d]	49	12	37	±	49	12	38	±	381611.175(100)	−55[d]
29	7	22	±	28	7	21	±	371983.664(100)	−30[d]	48	11	37	±	48	11	38	±	381776.255(100)	−22[d]
27	9	18	±	26	9	17	±	372023.715(100)	0[d]	47	10	37	±	47	10	38	±	381937.945(100)	−14[d]
26	10	16	±	25	10	15	±	372047.478(100)	14[d]	37	0	37	±	36	0	36	±	381994.645(100)	11[d]
25	12	14	±	24	12	13	±	372076.415(100)	−19[d]	36	1	35	±	35	1	34	±	382027.209(100)	20[d]
44	8	36	±	44	8	37	±	372090.431(100)	1[d]	35	3	33	±	34	3	32	±	382055.467(100)	6[d]
24	12	12	±	23	12	11	±	372115.003(100)	−8[d]	34	4	31	±	33	4	30	±	382080.114(100)	−5[d]
23	13	10	±	22	13	9	±	372173.642(100)	−2[d]	33	4	29	±	32	4	28	±	382101.929(100)	−23[d]
43	7	36	±	43	7	37	±	372234.967(100)	19[d]	32	5	27	±	31	5	26	±	382121.628(100)	−18[d]
22	15	8	±	21	15	7	±	372284.816(100)	48[d]	31	6	25	±	30	6	24	±	382139.978(100)	11[d]
15	9	6	±	14	7	7	±	372350.795(100)	−15[d]	30	7	23	±	29	7	22	±	382157.717(100)	14[d]
42	6	36	±	42	6	37	±	372376.197(100)	33[d]	29	9	21	±	28	9	20	±	382175.698(100)	−4[d]
21	16	6	±	20	16	5	±	372543.735(100)	−45[d]	28	10	19	±	27	10	18	±	382194.973(100)	−9[d]
21	15	6	±	20	15	5	±	372648.636(100)	127[d]	27	11	17	±	26	11	16	±	382216.811(100)	4[d]
20	19	2	±	19	19	1	±	372954.055(100)	18[d]	26	11	15	±	25	11	14	±	382243.069(100)	−7[d]
20	18	3	±	19	18	2	±	374443.006(100)	−26[d]	45	8	37	±	45	8	38	±	382251.225(100)	−5[d]
20	19	1	±	19	19	0	±	374471.704(100)	−1[d]	25	12	13	±	24	12	12	±	382277.144(100)	30[d]
17	17	0	±	16	15	1	±	376518.678(100)	17[d]	24	13	11	±	23	13	10	±	382326.179(100)	−20[d]
20	16	4	±	19	16	3	±	376748.015(100)	42[d]	44	7	37	±	44	7	38	±	382402.866(100)	49[d]
17	16	2	±	16	14	3	±	377946.318(100)	−70[d]	23	15	9	±	22	15	8	±	382410.158(100)	0[d]
65	28	37	±	65	28	38	±	378513.990(100)	−69[d]	43	6	37	±	43	6	38	±	382551.073(100)	36[d]
65	29	37	±	65	28	38	±	378514.040(100)	−24[d]	22	16	7	±	21	16	6	±	382597.685(100)	59[d]
17	14	3	±	16	12	4	±	378578.428(100)	−76[d]	22	15	7	±	21	15	6	±	382605.832(100)	−62[d]
64	28	37	±	64	27	38	±	378732.691(100)	−49[d]	21	17	5	±	20	17	4	±	382674.110(100)	50[d]
63	27	37	±	63	25	38	±	378948.115(100)	32[d]	42	6	37	±	42	5	38	±	382695.964(100)	−5[d]
62	25	37	±	62	25	38	±	379160.097(100)	22[d]	41	4	37	±	41	3	38	±	382837.502(100)	13[d]
60	23	37	±	60	23	38	±	379574.105(100)	58[d]	40	3	37	±	40	2	38	±	382975.665(100)	49[d]
59	22	37	±	59	22	38	±	379776.091(100)	77[d]	20	18	2	±	19	18	1	±	383023.958(100)	−35[d]
58	21	37	±	58	21	38	±	379974.606(100)	−25[d]	21	16	5	±	20	16	4	±	384028.346(100)	−38[d]
57	20	37	±	57	20	38	±	380169.997(100)	99[d]	20	17	3	±	19	17	2	±	386468.803(100)	19[d]
17	17	1	±	16	15	2	±	380354.884(100)	−44[d]	18	17	1	±	17	15	2	±	387004.760(100)	−20[d]
56	19	37	±	56	19	38	±	380361.742(100)	−71[d]	21	18	4	±	20	18	3	±	390677.882(100)	24[d]

[a] Transitions are assigned with the usual rotational quantum numbers and the ± sign, related to the tunneling component, of the upper and lower levels. [b] Obs is the observed frequency in MHz. The uncertainty is given in parentheses in kHz. [c] Diff is the observed minus calculated frequency in kHz corresponding to the constants in Table 10. [d] Transition from Breidung et al.[1] for which the tunneling splitting could not be resolved.

TABLE 10: Molecular Parameters Obtained for BF_2OH

parameter	value	parameter	value
A	10 320.462 1(9)	$h_2 \times 10^3$	−78.268 39(150)
B	10 099.393 3(9)		
C	5 095.135 27(120)	$h_{2k} \times 10^6$	−176.651(16000)
		$h_{2j} \times 10^6$	80.185(620)
$D_K \times 10^3$	10.798 567(4000)		
$D_{JK} \times 10^3$	−6.092 384(4000)	θ_2	88.589 194(400000)
$D_J \times 10^3$	7.056 963(1500)	ϕ_2	2.157 193(190000)
$\delta_K \times 10^3$	4.742 872(1400)		
$\delta_J \times 10^3$	3.152 228(420)		
$H_K \times 10^9$	78.061 7(66000)		
$H_{KJ} \times 10^9$	−17.959 4(170000)		
$H_{JK} \times 10^9$	−55.838 7(170000)		
$H_J \times 10^9$	26.222 8(13000)		
$h_K \times 10^9$	70.138 7(27000)		
$h_{KJ} \times 10^9$	−1.596 3(39000)		
$h_J \times 10^9$	12.936 8(8900)		

[a] All parameters are in MHz, except θ_2 and ϕ_2, which are in deg. Numbers in parentheses are one standard deviation in the same units as the last digit.

structural parameters introduced in section 4.1 were assumed to be independent of γ along the tunneling path. The two distances $R(BF_1)$ and $R(BF_2)$ were set to 131.79 pm, which is the average length of the two BF bonds for either equilibrium configurations. The six remaining structural parameters were set to the value displayed in Table 8 for the equilibrium configurations.

For the second tunneling path, which will be referred to as path II, the large-amplitude coordinate γ also increases from 0 to π. The path parametrization adopted is close to the MEP of section 2.2 and ensures that the molecule goes smoothly through the two equilibrium configurations and the intermediate configuration described in sections 2 and 4. For the angle α_1, the equation giving its numerical value in degrees is

$$\alpha_1(\gamma) = 120.82 \cos^2 \gamma + 121.60 \sin^2 \gamma \qquad (4)$$

and ensures that α_1 has the values displayed in Table 8 for $\gamma = 0$, $\pi/2$, and π. The angle α_2 was obtained from eq 4 using $\alpha_2(\gamma) = -\alpha_1(\gamma)$. Numerical values for the angles δ and θ(BOH) and for the distances R(BO) and R(OH) can be obtained using equations similar to eq 4. For the distance $R(BF_1)$, the equation giving its numerical value in pm is

$$R(BF_1)(\gamma) = 131.79 + 0.50 \cos \gamma - 0.09 \sin^2 \gamma \qquad (5)$$

TABLE 11: Numerical Values for θ_2 and ϕ_2[a]

path[b]	θ_2	ϕ_2	α[c]	Ω[d]
observed	88.589	2.157	225.685	176.912
path I	83.776	1.741	228.099	177.408
path II	81.158	1.910	229.405	177.098

[a] Numerical values are given in deg. [b] The path parametrization is given in this column. Observed indicates the experimental values retrieved in section 4.2; path I and path II refer to the paths described in section 4.3. [c] α is the angle between the rotation vector Ω and the *x*-axis (see text). [d] Ω is the angle of rotation (see text).

In agreement with Table 8, this equation ensures that the distance $R(BF_1)(\gamma)$ takes on three different values. The distance $R(BF_2)$ can be found from eq 5 using $R(BF_2)(\gamma) = R(BF_1)(\pi - \gamma)$.

Table 11 allows us to compare observed and calculated values for the angles θ_2 and ϕ_2. In addition to these angles, two angles, α and Ω, also appear in this table and have the following meaning. Keeping in mind that the angles θ_2 and ϕ_2 parametrize the rotation $S^{-1}(\phi_2 + \pi,\theta_2,\phi_2)$, the rotation vector Ω of this rotation lies in the *xz*-plane and the S^{-1} rotation can also be characterized by α, the angle between Ω and the *x*-axis, and by Ω, the angle of rotation which is also the length of Ω. Table 11 shows that the differences between path I and path II are small. The largest change is for α which undergoes a 1.3 increase. For both path I and path II, the agreement with the experimental values is fairly satisfactory. With path I the discrepancy between observed and calculated values of α is less than 3°. With path II, the agreement for α is not as good, but a very good value of Ω is obtained. This is not so surprising as path II is more realistic.

5. Discussion

Theoretical and experimental investigations of the torsional tunneling motion of the nonrigid BF_2OH molecule are reported in this paper. In the experimental investigation, the reported microwave measurements led to the first determination of the tunneling splitting in the ground vibrational state. In the theoretical investigation, aided by ab initio calculations, values for the tunneling splitting were calculated for four vibrational states using the MEP between the two planar equilibrium configurations of the molecule.

Tunneling splittings were calculated theoretically for the ground, 4^09^1, 4^09^2, and 4^19^0 vibrational states and are given in Table 6. For the two latter states, these theoretical values are in good agreement with the experimental ones.[8] The present theoretical calculation accounts, therefore, for the unexpectedly large value of the tunneling splitting in the 4^19^0 vibrational state, which is not an excited vibrational state of the torsional mode. For the ground vibrational state, the theoretical value is about 2.5×10^{-5} cm^{-1} = 0.75 MHz, which is in fairly good agreement with the experimental one, 0.156 MHz. Using the theoretically obtained MEP, the parameters corresponding to the rotational dependence of the tunneling splitting[24−26] were computed and found to be in satisfactory agreement with those obtained from the line frequency analysis. This comparison is displayed in Table 11. At last, for the 4^09^1 vibrational state, for which no splitting could be observed in the infrared spectra,[8] a value smaller than the experimental resolution is assumed for the tunneling splitting. This agrees well with a calculated value of 6×10^{-4} cm^{-1}.

Acknowledgment. The portion of this work in Austin was supported by grant F-100 from the Welch Foundation. We are grateful to Prof. John Stanton for permission to use his version of the ACES2-MAB program.

References and Notes

(1) Breidung, J.; Demaison, J.; D'Eu, J.-F.; Margulès, L.; Collet, D.; Mkadmi, E. B.; Perrin, A.; Thiel, W. *J. Mol. Spectrosc.* **2004**, *228*, 7−22.
(2) Jacox, M. E.; Irikura, K. K.; Thompson, W. E. *J. Chem. Phys.* **2000**, *113*, 5705.
(3) Collet, D.; Perrin, A.; Bürger, H.; Flaud, J.-M. *J. Mol. Spectrosc.* **2002**, *212*, 118.
(4) Perrin, A.; Cavajal-Zaera, M.; Dutkiewicz, Z.; Flaud, J.-M.; Collet, D.; Bürger, H.; Demaison, J.; Willaert, F.; Mäder, H.; Larsen, N. W. *Mol. Phys.* **2004**, *102*, 1641.
(5) Takeo, H.; Curl, R. H. *J. Chem. Phys.* **1972**, *56*, 4314.
(6) Vormann, K.; Dreizler, H. *Z. Naturforsch.* **1989**, *44A*, 1191.
(7) Petkie, D. T.; Helminger, P.; Behnke, M.; Medvedev, I. R.; De Lucia, F. C. *J. Mol. Spectrosc.* **2005**, *189*, 233.
(8) Perrin, A.; Bertseva, E.; Flaud, J.-M.; Collet, D.; Bürger, H.; Masiello, T.; Blake, T. A. *Mol. Phys.*, in press.
(9) Kohn, W.; Sham, L. J. *Phys. Rev. A* **1965**, *140*, 1133.
(10) Becke, A. D. *J. Chem. Phys.* **1993**, *98*, 5648.
(11) Lee, C.; Yang, W.; Parr, R. G. *Phys. Rev. B* **1988**, *37*, 785.
(12) Møller, C.; Plesset, M. S. *Phys. Rev.* **1934**, *46*, 618.
(13) Purvis, G. D., III; Bartlett, R. J. *J. Chem. Phys.* **1982**, *76*, 1910.
(14) Raghavachari, K.; Trucks, G. W.; Pople, J. A.; Head-Gordon, M. *Chem. Phys. Lett.* **1989**, *157*, 479.
(15) Molpro, version 2006.1, a package of ab initio programs. Werner, H.-J.; Knowles, P. J.; Lindh, R.; Manby, F. R.; Schütz, M.; P. Celani, T. K.; Rauhut, G.; Amos, R. D.; Bernhardsson, A.; Berning, A.; Cooper, D. L.; Deegan, M. J. O.; Dobbyn, A. J.; Eckert, F.; Hampel, C.; Hetzer, G.; Lloyd, A. W.; McNicholas, S. J.; Meyer, W.; Mura, M. E.; Nicklass, A.; Palmieri, P.; Pitzer, R.; Schumann, U.; Stoll, H.; Stone, A. J.; Tarroni, R.; Thorsteinsson, T. http://www. molpro. net, 2006.
(16) Stanton, J. F.; Gauss, J.; Watts, J. D.; Lauderdale, W. J.; Barlett, R. J. *Int. J. Quantum Chem. Symp.* **1992**, *26*, 879.
(17) Dunning, T. H., Jr. *J. Chem. Phys.* **1989**, *90*, 1007.
(18) Bak, K. L.; Gauss, J.; Jørgensen, P.; Olsen, J.; Helgaker, T.; Stanton, J. F. *J. Chem. Phys.* **2001**, *114*, 6548.
(19) Bersuker, I. B. *Chem. Rev.* **2001**, *101*, 1067.
(20) Bersuker, I. B. *The Jahn-Teller Effect*; Cambridge University Press: New York, 2006.
(21) Lanczos, C. *J. Res. Natl. Bur. Stand.* **1950**, *45*, 255.
(22) Krüger, M.; Harder, H.; Gerke, C.; Dreizler, H. *Z. Naturforsch.* **1993**, *48A*, 737−738.
(23) Gerke, C. Unpublished results, Kiel.
(24) Hougen, J. T. *J. Mol. Spectrosc.* **1985**, *114*, 395−426.
(25) Coudert, L. H.; Hougen, J. T. *J. Mol. Spectrosc.* **1988**, *130*, 86−119.
(26) Coudert, L. H.; Hougen, J. T. *J. Mol. Spectrosc.* **1990**, *139*, 259−277.
(27) Coudert, L. H.; Perrin, A. *J. Mol. Spectrosc.* **1995**, *172*, 352−368.
(28) Paulse, C. D.; Coudert, L. H.; Goyette, T. M.; Crownover, R. L.; Helminger, P.; Lucia, F. C. D. *J. Mol. Spectrosc.* **1996**, *177*, 9−18.